

†Supporting Information
for
Soft chemical *in-site* synthesis, formation mechanism and
electrochemical performances of 1D bead-like AgVO₃
nanoarchitectures

Xingang Kong^a, Zhanglin Guo^a, Chaobin Zeng^a, Jianfeng Huang^{a*}, Liyun Cao^a, Li Li^a, Lixiong Yin^a,

Puhong Wen^b, Qi Feng^c, Zhanwei Xu^{a*}

^a School of Materials Science and Engineering, Shaanxi University of Science and Technology,
Weiyang, Xi'an, Shaanxi 710021, PR China

^b Department of Chemistry and Chemical Engineering, Baoji University of Arts and Science, 1 Gaoxin
Road, Baoji, Shaanxi 721013, PR China

^c Department of Advanced Materials Science, Faculty of Engineering, Kagawa University, 2217-20
Hayashi-cho, Takamatsu-shi, 761-0396 Japan

*Author to whom correspondence should be addressed. E-mail: huangjf@sust.edu.cn,

davidemt@126.com

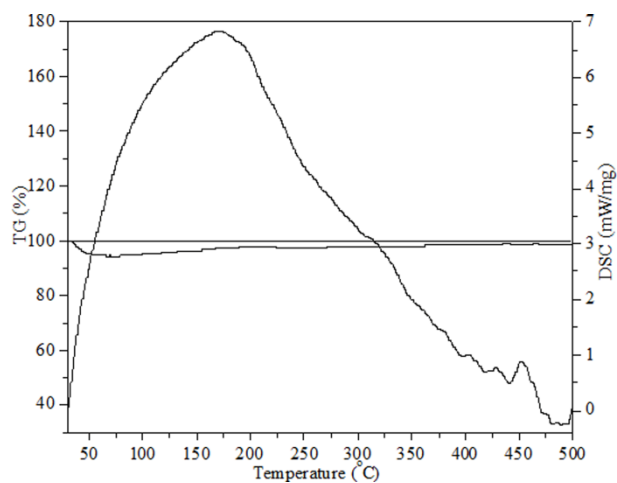


Fig. S1 TG-DTA curves of the α -AgVO₃ product obtained by the treatment of K₂V₆O₁₆·2.7H₂O precursor in AgNO₃ water solution at room-temperature for 24h.

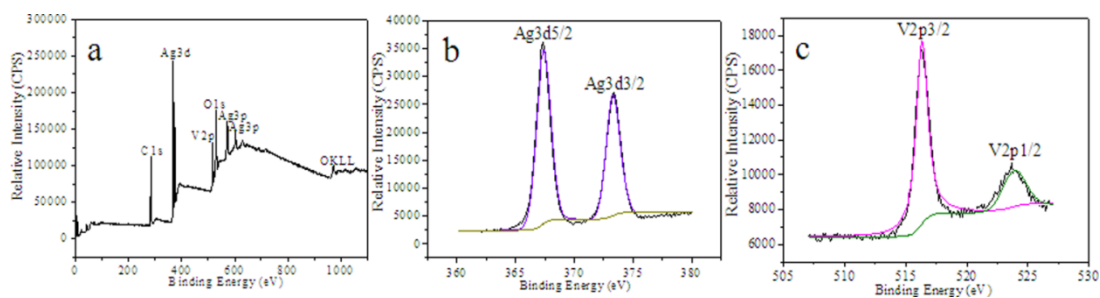


Fig. S2 XPS spectra of the β -300 nanoarchitectures. (a) XPS survey spectrum of the sample, (b) XPS spectrum of the Ag 3d region, (c) XPS spectrum of the V 2p region.

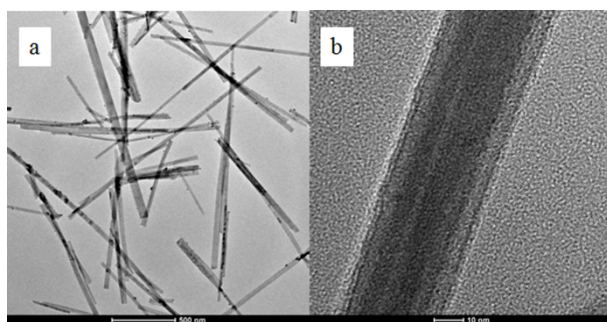


Fig. S3 TEM and HRTEM images of β -AgVO₃ nanowires sample obtained by the literature's method.

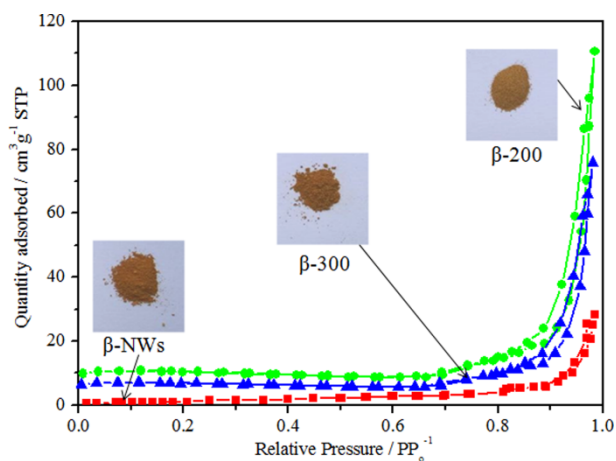


Fig. S4 Nitrogen adsorption/desorption isotherms and photos of the β -200, β -300 nanoarchitectures and β -AgVO₃ nanowires samples, respectively.

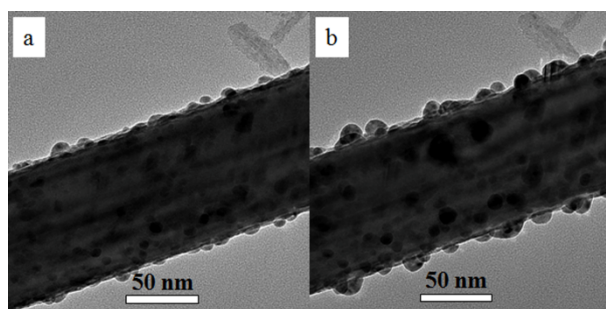


Fig. S5 TEM images of the K₂V₆O₁₆·2.7H₂O/ α -AgVO₃ composite fiber under exposure to electron beam. The size α -AgVO₃ nanoparticles increased after an exposure time of about 20 seconds.

	Time	pH Value
0.5M AgNO ₃ solution	0.5M AgNO ₃ solution	5.70
0.5M AgNO ₃ solution+K ₂ V ₆ O ₁₆ ·2.7H ₂ O	1 min	4.72
0.5M AgNO ₃ solution+K ₂ V ₆ O ₁₆ ·2.7H ₂ O	15 min	4.27
0.5M AgNO ₃ solution+K ₂ V ₆ O ₁₆ ·2.7H ₂ O	30 min	4.13
0.5M AgNO ₃ solution+K ₂ V ₆ O ₁₆ ·2.7H ₂ O	1 h	4.11
0.5M AgNO ₃ solution+K ₂ V ₆ O ₁₆ ·2.7H ₂ O	2 h	3.82
0.5M AgNO ₃ solution+K ₂ V ₆ O ₁₆ ·2.7H ₂ O	4 h	3.70
0.5M AgNO ₃ solution+K ₂ V ₆ O ₁₆ ·2.7H ₂ O	12 h	2.76
0.5M AgNO ₃ solution+K ₂ V ₆ O ₁₆ ·2.7H ₂ O	18 h	2.28
0.5M AgNO ₃ solution+K ₂ V ₆ O ₁₆ ·2.7H ₂ O	24 h	2.21

Tab. S1 Temporal evolution pH value of the system of K₂V₆O₁₆·2.7H₂O treated in 0.5M AgNO₃ solution.

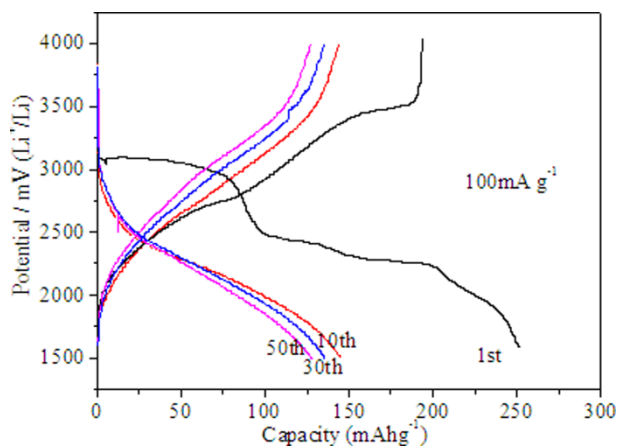


Fig. S6 The charge/discharge profiles under different cycles of β -300 sample at current density of 100 mA g^{-1} .

Fig. S6 depicts the charge/discharge profiles under different cycles of β -300 sample at 1st, 10th, 30th and 50th cycle at current density of 100 mA g^{-1} . The initial discharge capacity was found to be 251 mA h g^{-1} at a current density of 100 mA g^{-1} . It clearly shows in Fig. S6 that the initial capacity decreased significantly with increasing cycling. The length of plateau (at ca. 2.5 V) becomes shorter and tends to disappear, indicating that the insertion of Li ion into the matrix of β -300 becomes more and more difficult and tends to lose activity¹. As depicted in Fig. R2, the capacity decreased in few initial cycles and dropped significantly to 141 mAh g^{-1} after 10 cycles, indicating that the electrode made of β -300 nanoarchitectures is unstable. From the 10th cycle to 50th cycle, the capacity has only slightly decrease, from 141 to 127 mAh g^{-1} , which indicates that the β -300 electrode possesses good cycling stability.¹

Materials content	Synthesis method	Structure	Capacity (mA h g ⁻¹)	Current density	References
β -AgVO ₃ -300	Soft chemical <i>in-situ</i> synthesis	bead-like nanoarchitectures	251(initial) 127(50)	100 mA g ⁻¹	This work
β -AgVO ₃	Hydrothermal	radial nanowire clusters	200(initial) 68(50)	20 mA g ⁻¹	Han et. al ²
β -AgVO ₃	Hydrothermal	radial nanowire clusters	167(initial) 70(50)	50 mA g ⁻¹	Han et. al ²
β -AgVO ₃	Hydrothermal	radial nanowire clusters	220(initial) 90(50)	100 mA g ⁻¹	Han et. al ²
β -AgVO ₃	Hydrothermal	radial nanowire clusters	163(initial) 95(50)	500 mA g ⁻¹	Han et. al ²
AgVO ₃ /graphene	<i>in situ</i> Hydrothermal	3D porous composite aerogels	163(initial) 125(50)	100 mA g ⁻¹	Liang et. al ³
Ag/AgVO ₃	solid-state approach	nanorods	242.5(initial) 111(30)	50 mA g ⁻¹	Liang et. al ⁴
Ag/AgVO ₃ /CNTs	Hydrothermal	3D self-bridged networks	285 (initial) 52(20)	50 mA g ⁻¹	Liang et. al ⁵
β -AgVO ₃	Hydrothermal	nanowires	302.1(initial) 90.6 (20)	0.01 mA	Zhang et. al ⁶
β -AgVO ₃	Hydrothermal	nanowires	104(initial)	0.1mA cm ⁻²	Rout et. al ⁷
AgVO ₃ -PANI	<i>in situ</i> chemical oxidative polymerization	triaxial nanowires	211(initial) 131 (20)	30 mA g ⁻¹	Mai et. al ⁸

Tab. S2 Discharging capacity performance comparison of β -AgVO₃-300 electrode with recently reported β -AgVO₃ electrodes.

Tab. S2 lists the electrochemical performance of previous reported silver vanadium oxides (SVOs) and our results, which has been added into Supporting Information. As shown in Tab. S2, our AgVO₃ electrodes have high capacity and good cycle stability. Both the initial capacity and capacity of cycled for 50 cycles in our work are higher than that of hydrothermal synthesized AgVO₃/graphene reported by Liang et. al.³, but the latter has better cycling stability than that of ours. The great cycling stability of AgVO₃/graphene is benefited from its 3D porous network with improved electrical conductivity and fast charge transport compared with pure β -AgVO₃ sample. The initial capacities of Ag/AgVO₃ obtained by solid state approach⁴ and β -AgVO₃ prepared via hydrothermal method⁶ are very high when tested at lower current densities.

Han et. al.² prepared radial β -AgVO₃ nanowire clusters on ITO and this moundlily like β -AgVO₃ nanowires show high discharge capacity and excellent cycling stability at high-rate discharge, which

may be mainly attributed to the effect of reduced self-aggregation.² In our work, the unique 1D bead-like β - AgVO_3 nanoarchitectures can also efficiently resist the self-aggregation of β - AgVO_3 nanoparticles thus the 1D bead-like β - AgVO_3 nanoarchitectures possesses high capacity and good cycling ability.

Recently, some 3D structures based on β - AgVO_3 have been reported, for example, $\text{AgVO}_3/\text{graphene}$ composite prepared by Liang et. al³, $\text{Ag}/\text{AgVO}_3/\text{CNTs}$ by Liang et. al⁵, silver vanadium oxides/polyaniline (SVO/PANI) tri-axial nanowires by Mai et al⁸. All the electrodes show great electrochemical properties with a higher initial capacity and better cycle stability than the pure β - AgVO_3 nanowires. And the higher initial capacity and better cycle stability are the results of effective charge transport and improved electrical conductivity.

In our work, the unique bead-like structure and little particle size can improve the charge transport because the distance of charge transfer can be largely shortened. At the same time, the unique bead-like structure can efficiently resist the self-aggregation of β - AgVO_3 nanoparticles, which is also beneficial to the enhancement of the capacity and the improvement of cycling ability.

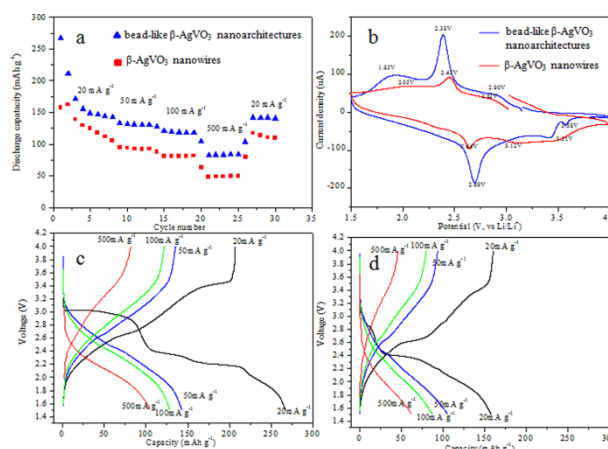


Fig. S7 Rate capability (a) and CV curves (b) of the β -300 nanoarchitectures and β - AgVO_3 nanowires samples, Galvanostatic charge/discharge curves of β -300 nanoarchitectures (c) and of β - AgVO_3

nanowires samples (d).

Fig. S7a shows the rate capabilities of the bead-like β -300 nanoarchitectures sample compared to the β -NWs sample. The specific capacity of the two samples both present the decreasing trend, as the current densities increase from $20 \text{ mA}\cdot\text{g}^{-1}$ to $500 \text{ mA}\cdot\text{g}^{-1}$. At the current density of $20 \text{ mA}\cdot\text{g}^{-1}$ after 5 cycles, the β -300 and the β -NWs sample show capacities of $147, 105 \text{ mAh}\cdot\text{g}^{-1}$, respectively. At $50 \text{ mA}\cdot\text{g}^{-1}$ after 5 cycles, they display $128, 99 \text{ mAh}\cdot\text{g}^{-1}$, respectively. At $100 \text{ mA}\cdot\text{g}^{-1}$ after 5 cycles, the β -300 and the β -NWs sample are $119, 81 \text{ mAh}\cdot\text{g}^{-1}$. At a high current density of $500 \text{ mA}\cdot\text{g}^{-1}$, these values are $83, 50 \text{ mAh}\cdot\text{g}^{-1}$ after 5 cycles. When the current density is returned to $20 \text{ mA}\cdot\text{g}^{-1}$, after 5 cycles, the β -300 nanoarchitectures and the β -NWs sample are $147, 105 \text{ mAh}\cdot\text{g}^{-1}$. It is appear that the bead-like β -300 nanoarchitectures clearly displays better performance at the current densities range from 20 to $500 \text{ mA}\cdot\text{g}^{-1}$. The phenomenon may be attributed to the main reason that the β -300 nanoarchitectures possess the larger surface area than that of the β -NWs, meaning the more effective contact areas of active materials, conductive additives, and shorter lithium ion diffusion paths^{9,10}.

Cyclic voltammograms (CVs) of the electrodes made from the as prepared β -300 nanoarchitectures and β -NWs in the first cycle at a scan rate of 0.1 mV s^{-1} in a potential window of 4-1.5 V (vs. Li^+/Li). The CV curves are shown in Fig. S7b, with maximum of each peak being labeled on the figure. The shapes of the CV curves of the electrodes are quite similar. The positions of the sloping plateaus (Fig. S7c and d) roughly agree with the CV results.

The β -300 electrode (Fig. S7b), in the cathodic polarization process, three peaks were observed at around 3.58, 3.43, and 2.69 V versus Li^+/Li , corresponding to the complicated multistep electrochemical lithium intercalation processes; while in the following anodic polarization, three characteristic peaks were located at 2.90, 2.38 and 1.85 V, corresponding to the lithium extraction

processes. Combining with the Galvanostatic charge/discharge curve (Fig. S7c), we can index the three cathodic peaks to the corresponding reduction reactions. The peak at 3.58 V is assigned to silver reduction from Ag^+ to Ag^0 , and the peak at 3.43 V corresponds to dominant reduction from V^{5+} to V^{4+} and partial reduction from V^{4+} to V^{3+} , whereas the peak at 2.69 V is in agreement with further reduction of vanadium from V^{4+} to V^{3+} and Ag^+ to Ag^0 , all of which are similar to other reports.^{1, 3-6} In CV curves of the two electrodes (Fig. S7b), there are differences in the positions of the reduction and oxidation peaks, but the shapes are similar, indicating the same electrochemical reactions.^{3, 5}

Fig. S7c presents the first charge/discharge profiles of the β -300 electrodes cycled at current densities from 20 to 500 $\text{mA}\cdot\text{g}^{-1}$. The initial discharge and charge capacities at 20 $\text{mA}\cdot\text{g}^{-1}$ are 267 and 208 $\text{mAh}\cdot\text{g}^{-1}$, respectively. With increasing of the charge/discharge rates, the potential differences between charge and discharge plateaus exhibit a tendency to increase which could be attributed to the increased electrode polarization and the sluggish diffusion kinetics of Li-ion at high rates.¹¹ Fig. S7d gives the first charge/discharge profiles of the β -NWs electrodes cycled at current densities from 20 to 500 $\text{mA}\cdot\text{g}^{-1}$. The initial discharge and charge capacities at 20 $\text{mA}\cdot\text{g}^{-1}$ are 158 and 160 $\text{mAh}\cdot\text{g}^{-1}$, respectively. The β -300 cathode shows the higher first discharge capacity at various current densities than that of β -NWs cathode. These results are in accordance with that of specific capacities of samples tested at different rates (Fig. S7a).

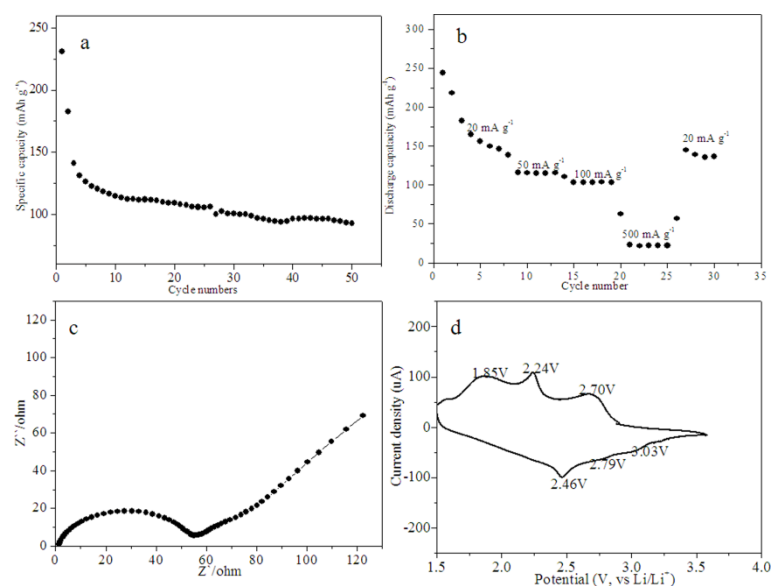


Fig. S8 Cycling performance, tested at 100 mA g^{-1} (a), rate capability(b), Nyquist plot(c) and CV curve(d) of β -200 sample

In Fig. S8a, the initial capacity of the bead-like β -200 nanoarchitectures sample is $231 \text{ mAh}\cdot\text{g}^{-1}$, yielding a reversible capacity $122 \text{ mAh}\cdot\text{g}^{-1}$ after 6 cycles. Its capacity decreases to $93 \text{ mAh}\cdot\text{g}^{-1}$ after 50 cycles under the current density of $100 \text{ mA}\cdot\text{g}^{-1}$, and its capacity fading per cycle from 6th to 50th is 0.66%. Fig. S8b shows the rate capabilities of β -200 sample. The specific capacity presents the decreasing trend, as the current densities increase from $20 \text{ mA}\cdot\text{g}^{-1}$ to $500 \text{ mA}\cdot\text{g}^{-1}$. At the current density of $20 \text{ mA}\cdot\text{g}^{-1}$ after 5 cycles, the β -200 sample shows capacity of $138 \text{ mAh}\cdot\text{g}^{-1}$. At $50 \text{ mA}\cdot\text{g}^{-1}$ after 5 cycles, the capacity is $116 \text{ mAh}\cdot\text{g}^{-1}$. At $100 \text{ mA}\cdot\text{g}^{-1}$ after 5 cycles, the capacity is $103 \text{ mAh}\cdot\text{g}^{-1}$. At a high current density of $500 \text{ mA}\cdot\text{g}^{-1}$, the value is only $22 \text{ mAh}\cdot\text{g}^{-1}$ after 5 cycles, much less than those of β -300 and β -NWs sample. When the current density is returned to $20 \text{ mA}\cdot\text{g}^{-1}$, after 5 cycles, the capacity of β -200 is $136 \text{ mAh}\cdot\text{g}^{-1}$.

Comparing performance of the β -200 and β -300 sample, we can find that the β -200 shows worse property than that of β -300 sample. The reason may be that the β -200 sample contains a small quantity of α - AgVO_3 , which may decrease its capacity and cycling performance. In addition, the crystallinity of

β -200 is lower than that of β -300 sample(Fig. 1) that may affect the cycling stability and the capacity of high current density because long-time cycling and high current density lead to the destruction of the crystal structure.⁹

The Nyquist plot(Fig. S8c), is composed of a depressed semicircle in the high-frequency region and an oblique line with an angle near 45° relative to the real axis in the low-frequency region. At high frequency range, a smaller diameter of the semicircle represents smaller charge transfer impedance the charge transfer resistance.¹⁰ Among the β -200, β -300 and β -NWs samples, the β -200 sample has the smallest charge transfer impedance(Fig. S8c and Fig. 10) for its smallest diameter. This result fits well with the specific surface area(Fig. S4) of these three samples and a direct consequence of morphology difference between the bead-like nanostructures and β -NWs². In addition, the β -200 demonstrate a shorter Warburg region than that of the β -NWs sample, which is expected due to the smaller particle size resulting markedly smaller diffusion lengths in the former.¹²

The β -200 show a similar CV curve with that of β -300 electrode, which indicates that they have the same electrochemical reactions. The β -200 electrode (Fig. S8d), in the cathodic polarization process, three peaks were observed at around 3.03, 2.79, and 2.46 V versus Li^+/Li , corresponding to the complicated multistep electrochemical lithium intercalation processes; while in the following anodic polarization, three characteristic peaks were located at 2.70, 2.24 and 1.85 V, corresponding to the lithium extraction processes. We can index the three cathodic peaks to the corresponding reduction reactions. The peak at 3.03 V is assigned to silver reduction from Ag^+ to Ag^0 , and the peak at 2.79 V corresponds to dominant reduction from V^{5+} to V^{4+} and partial reduction from V^{4+} to V^{3+} , whereas the peak at 2.46 V is in agreement with further reduction of vanadium from V^{4+} to V^{3+} and Ag^+ to Ag^0 , all of which are similar other reports.³⁻⁶

References

- [1] Z. Chen, S. Gao, R. Li, M. Wei, K. Wei and H. Zhou, *Electrochim. Acta*, 2008, **53**, 8134.
- [2] C. Han, Y. Pi, Q. An, L. Mai, J. Xie, X. Xu, L. Xu, Y. Zhao, C. Niu, A. Khan and X. He, *Nano Lett.*, **2012**, *12*, 4668.
- [3] L. Liang, Y. Xu, Y. Lei and H. Liu, *Nanoscale*, 2014, **6**, 3536.
- [4] S. Liang, J. Zhou, A. Pan, X. Zhang, Y. Tang, X. Tan and R. Wu, *J. Power Sources*, 2013, **228**, 178.
- [5] L. Liang, H. Liu and W. Yang, *Nanoscale*, 2013, **5**, 1026.
- [6] S. Zhang, W. Li, C. Li and J. Chen, *J. Phys. Chem. B*, 2006, **110**, 24855.
- [7] C. Rout, U. Gautam, Y. Bando, D. Rangappa, X. Fang, L. Li and D. Golberg, *Sci. Adv. Mater.*, 2010, **2**, 407.
- [8] L. Mai, X. Xu, C. Han, Y. Luo, L. Xu, Y. Wu and Y. Zhao, *Nano Lett.*, 2011, **11**, 4992.
- [9] Shen Y.; Eltzholtz, J.; Iversen, B.; *Chem. Mater.* **2013**, *25*, 5023.
- [10] Bao, Q.; Bao, S.; Li, C.; Qi, X.; Pan, C.; Zang, J.; Wang, W.; Tang, D.; *Chem. Mater.* **2007**, *19*, 5965.
- [11] T. Yi, Z. Fang, Y. Xie, Y. Zhu and S. Yang, *ACS Appl. Mater. Inter.*, 2014, **6**, 20205.
- [12] Xu, Z.; Wang, H.; Li, Z.; Kohandehghan, A.; Ding, J.; Chen, J.; Cui, K.; Mitlin, D. *J. Phys. Chem. C*, **2014**, *118*, 18387.